RSC Applied Interfaces

ROYAL SOCIETY OF CHEMISTRY

REVIEW

View Article Online
View Journal | View Issue

Cite this: *RSC Appl. Interfaces*, 2026, 3, 9

Bioinspired smart slippery surfaces for bubble manipulation: from fundamental principles to emerging applications

Duanqiang Shi,†[a] Pu Guo,†[b] Yang Liu,[a] Xiaoxiao Zhou,[a] Shuchun Jiang,[a] Zubin Wang *[a] and Qun Xu *[ac]

Received 22nd September 2025,
Accepted 6th November 2025

DOI: 10.1039/d5lf00281h

rsc.li/RSCApplInter

Controllable bubble manipulation on functional surfaces plays a significant role in fundamental research and emerging applications. Inspired by the *Nepenthes* pitcher plant, smart slippery surfaces have emerged as a promising platform for bubble manipulation thanks to their unique bubble adhesion behaviors. This review paper presents a comprehensive summary of the advancement in bioinspired smart slippery surfaces for bubble manipulation. It first provides the design principles and bubble manipulation mechanisms of smart slippery surfaces. Then, it highlights different bubble manipulation strategies, encompassing passive and active modes under various external stimuli. Furthermore, the emerging bubble-related applications of smart slippery surfaces, such as bubble collectors, bubble microreactors, optical shutters, and bubble microrobots are systematically summarized. Finally, it discusses the limitations and provides some future perspectives regarding smart slippery surfaces for bubble manipulation.

1. Introduction

Controllable bubble manipulation has aroused extraordinary interest due to its immense potential in diverse application areas, such as mineral flotation, nanogenerator, heat transfer of boiling water, water treatment, gas-involved catalytic reaction, *etc.*[1–8] Achieving precise bubble manipulation requires meticulous tailoring of functional surfaces' wettability and micro/nanostructures.[9–14] Inspired by the phenomenon of water spider hiding underwater,[15,16] superaerophilic surfaces, which allow gas to be readily trapped within their micro/nanostructures, are taken for reliable gas suppliers in aqueous media.[17–19] In contrast, the superaerophobic surfaces—featuring ultralow bubble adhesion—can rapidly remove bubbles from the surfaces.[20–22] Although these superaerophilic and superaerophobic surfaces hold significant importance for

[a] *School of Materials Science and Engineering, Zhengzhou University, Zhengzhou 450001, PR China. E-mail: wangzb@zzu.edu.cn, qunxu@zzu.edu.cn*
[b] *Shaanxi Key Laboratory of Liquid Crystal Polymer Intelligent Display, Key Laboratory of Liquid Crystal Polymers based Flexible Display Technology in National Petroleum and Chemical Industry, Technological Institute of Materials & Energy Science (TIMES), Xijing University, Xi'an, 710123, PR China*
[c] *Henan Institute of Advanced Technology, Zhengzhou University, Zhengzhou 450003, PR China*
† These authors contributed equally to this work.

Duanqiang Shi

Duanqiang Shi is currently a master student at the School of Materials Science and Engineering, Zhengzhou University. He received his bachelor's degree from Henan Polytechnic University in 2021. His current research interest is controllable fluid transportation on slippery surfaces.

Pu Guo

Pu Guo is currently an Assistant Professor at Xijing University. She obtained her PhD degree from Beihang University in 2024. Her current research interest is preparation and application of durable slippery surfaces.

static bubble manipulation, they face inherent limitations in dynamic case. (i) Superaerophilic surfaces with gas spreading properties are not suitable for manipulating discrete bubbles. (ii) Superaerophobic surfaces with low bubble adhesion must be positioned above the bubbles to counteract buoyancy-induced detachment.[23] (iii) High-pressure environments would lead to water or gas infiltrate surface micro/nanostructures, compromising their superaerophilicity or superaerophobicity and disabling bubble manipulation.[24,25] (iv) Fragile micro/nanostructures are vulnerable to damage under complicated underwater conditions.[26,27]

Nature often provides ingenious solutions to complex conundrums, and underwater bubble manipulation is no exception. Inspired by the exceptional liquid repellency of the slippery peristomes of *Nepenthes* pitcher plants, Aizenberg and co-workers in 2011 pioneered the prototype of a slippery liquid infused porous surface (thereafter referred to as a slippery surface).[28] Slippery surfaces are prepared by infusing inert lubricants into porous network substrates.[28–33] Unlike the conventional superwetting surfaces, slippery surfaces demonstrate state-of-the-art self-healing properties and compression resistance because of the fluidity, reconfigurability, and incompressibility of the lubricants.[28,34–38] More spectacularly, slippery surfaces feature ultralow lateral adhesion and moderate normal adhesion, distinct traits absent in conventional superwetting (superaerophilic and superaerophobic) surfaces. These unique adhesion behaviors make them the ideal choice for underwater bubble manipulation.[25,39–42] In 2017, Yu *et al.* first introduced slippery surfaces into bubble manipulation, demonstrating a high normal bubble adhesion of ~300 μN and an ultralow bubble sliding angle of <5°, successfully achieving point-to-point bubble delivery.[43] Given the importance of functional surfaces with controllable bubble manipulation capacity in fundamental research and intelligent applications, smart slippery surfaces are creatively proposed by incorporating responsive substrates and lubricants. To this end, in 2019, our group constructed a magnetic slippery gel surface, enabling controllable bubble sliding on a tilted surface by reversibly regulating the bubble's lateral adhesion.[44] In the same year, Chen *et al.* achieved photothermal actuation of bubbles on a slippery surface by overcoming lateral bubble adhesion.[45] Subsequently, a plethora of smart slippery surfaces, including magnetic, photothermal, mechano-stretching, and temperature-responsive types, have been developed to manipulate bubbles by switching or overcoming bubble adhesion under external stimuli.[44–47] Based on their controllable bubble manipulation capacity, smart slippery surfaces have inspired a host of emerging applications, including smart bubble collectors, bubble microreactors, optical shutters, and bubble microrobots.[44–47]

To the best of our knowledge, many excellent reviews have summarized the progress of bubble manipulation on superwetting surfaces, *i.e.*, superaerophilic and superaerophobic surfaces, and stimuli-responsive surfaces.[9,48,49] However, recent advances of bubble manipulation on smart slippery surfaces have not been fully reviewed. Taking into consideration the critical importance of bubble manipulation across diverse fields, in this review, we mainly focus on the major advancements in bubble manipulation on smart slippery surfaces. After a succinct introduction to the design principles of slippery surfaces for bubble manipulation, we discuss the underlying mechanisms of passive control and active actuation of bubbles. We then systematically delve into the passive control and active actuation of bubbles under external stimuli, such as magnetic field, photothermal field, mechanical stretching, temperature field, photopyroelectric field, *etc.* After that, we highlight the emerging applications related to bubble manipulation across various domains, such as gas collectors,

Zubin Wang

Zubin Wang is currently an Assistant Professor at the School of Materials Science and Engineering, Zhengzhou University. He obtained his PhD degree from Beihang University in 2020. His scientific interest focuses on bioinspired interface materials for controllable fluid transportation and applications.

Qun Xu

Qun Xu is currently a full professor at Zhengzhou University. Qun Xu is a full professor in the Henan Institute of Advanced Technology, the College of Materials Science and Engineering, Zhengzhou University. She obtained her PhD in Physical Chemistry from the Institute of Chemistry, Chinese Academy of Science in 1999. And in 2001, she finished her post doctor work in the Karlsruhe Nuclear Center in Germany and returned back to China. Currently, she focuses on the design, synthesis and performance exploration of novel nanostructures with the assistance of supercritical CO_2.

microreactors, optical shutters, and bubble microrobots. Finally, we present an insight of the current challenges and forward-looking perspectives of smart slippery surfaces for bubble manipulation.

2. Design principles and manipulation mechanism

2.1. Design principles of slippery surfaces for bubble manipulation

Like the slippery peristomes of *Nepenthes* pitcher plants,[50,51] slippery surfaces typically consist of two key components: a porous substrate and an inert lubricant (Fig. 1a).[28] With advancements in nano-processing technologies, various porous films, including polymers,[52–54] ceramics,[55,56] metals,[57–59] and composites,[60,61] have been tailored as the substrates. Meanwhile, a wide array of inert liquids have been selected to serve as lubricants, such as DuPont Krytox oils,[28] fluorocarbon (FC-70, FC-40),[28,62] perfluoropolyether,[63] silicone oils,[35,44] liquid crystals,[54,64,65] ionic liquids,[66] hydroxylated polydimethylsiloxane (PDMS),[67] and olive oil.[68] During the preparation of slippery surfaces, infusing these lubricants into the porous substrates can form a molecularly smooth layer.

When used underwater for manipulating bubbles, a slippery surface may present three wetting configurations: the lubricant substituted with an ambient liquid, failing to repel bubbles (Fig. 1b-i); lubricant is substituted with a bubble, failing to manipulate bubbles (Fig. 1b-ii); a stable state with a continuous lubricant layer between the bubble and substrate (Fig. 1b-iii). To stably manipulate bubbles underwater, the following design principles for slippery surface must be satisfied:[28,69] (i) the lubricants must be absorbed into the porous films or swell into the gel substrates; (ii) the lubricants and the ambient liquid must be immiscible and chemically inert; (iii) the porous substrates must be more easily wetted by the lubricants than by the gas bubble and ambient liquid. To meet the first principle, porous or flat substrates must feature strong affinity to the lubricant, facilitating the wicking of lubricants. For the second principle, suitable lubricants should be carefully selected according to the predetermined ambient liquids. The third principle requires modifying the substrates' wettability to meet two prerequisites: (a) repelling ambient liquid (lipophilic under an ambient liquid) to guarantee the substrates preferentially wetted by the lubricant; (b) ensuring that the lubricant cannot be substituted by the gas bubble under an ambient liquid. When the above three criteria are satisfied, slippery surfaces can effectively manipulate bubbles underwater.

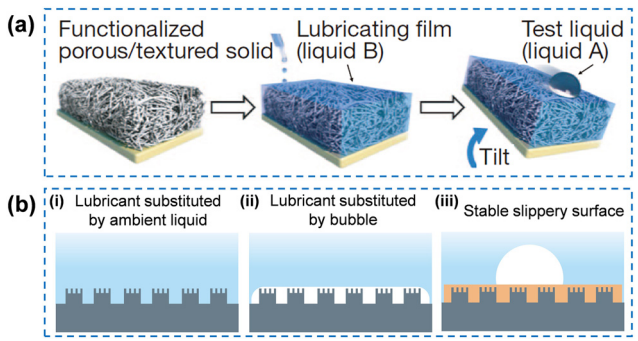

Fig. 1 (a) The preparation of a slippery surface. Reproduced with permission from ref. 28; copyright 2011, Springer Nature. (b) Schematic demonstration of various configurations: (i) the lubricant is substituted with an ambient liquid (the substrate is fully wetted by the ambient liquid), (ii) the lubricant is substituted with a bubble (the substrate is fully wetted by the bubble), and (iii) the bubble on a stable slippery surface.

2.2. Bubble manipulation mechanisms

On smart slippery surfaces, the forces acting on bubbles could be dynamically adjusted under external stimuli. From the perspective of force changes, bubble manipulation can be categorized into passive control and active actuation. As shown in Fig. 2a, when a bubble is deposited on a tilted surface (tilted angle of α), it experiences buoyancy (F_b), which can be divided into the two components: $F_{//}$ (parallel to the surface) and $F_\perp$ (vertical to the surface).[44] $F_{//}$ and $F_\perp$ can be calculated as: $F_{//} = \rho g V \sin\alpha$ and $F_\perp = \rho g V \cos\alpha$, respectively, where ρ, g and V denote the density of the ambient liquid, gravitational acceleration, and bubble volume, respectively. Moreover, the bubble is subjected to a normal adhesion force (F_d) and a lateral adhesion force (f). If the slippery surface initially assumes a slippery state, when the $F_{//}$ is larger than f, the bubble would slide upward on the tilted surface. When external stimuli increase f beyond $F_{//}$, the slippery surface turns to a non-slippery state, pinning the

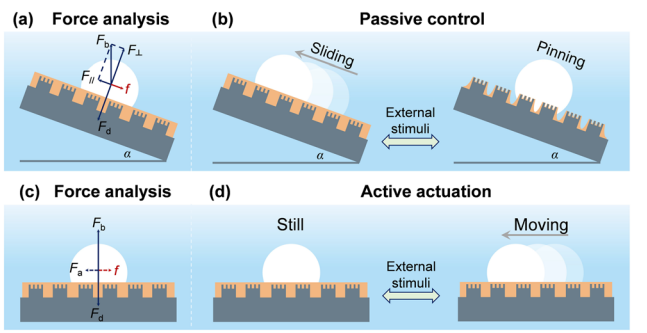

Fig. 2 Underlying mechanisms for manipulating bubbles on smart slippery surfaces. (a) Schematic demonstration of force analysis of a bubble on a tilted slippery surface. When $F_{//} > f$, bubbles could slide off the surface. Once $F_{//} < f$, bubbles would be pinned on the surface. (b) Passive control of bubbles by switching the slippery surfaces between the low adhesion state and high adhesion state under external stimuli. (c) Schematic demonstration of the force analysis of a bubble on a horizontal slippery surface. Under external stimuli, when the actuation force F_a exceeds the adhesion force ($F_a > f$), the bubble would move on the surface. (d) Active actuation of bubbles by overcoming adhesion between the bubble and surface under external stimuli.

bubble (Fig. 2b). Removing the stimuli restores the slippery state, which allows the bubble to slide again, achieving the passive control of the bubble. Conversely, if the surface originally occupies the non-slippery state (*i.e.* $F_{//} < f$), the bubble would be pinned on the slope. Exerting external stimuli to decrease the f ($< F_{//}$) would enable the bubble sliding. Removing the external stimuli would pin the bubble again. This demonstrates passive bubble manipulation by regulating lateral adhesion.

In the horizontal case, a bubble experiences only F_b and F_d (Fig. 2c). Due to the lack of actuation force, the bubble keeps stationary. To actuate the bubble, external stimuli are needed to produce actuation force (F_a). When F_a exceeds f, the bubble moves, achieving active actuation. Withdrawing the stimuli removes F_a, and the bubble stops due to f. Thus, the active actuation of the bubble can be carried out by overcoming the lateral adhesion. Notably, a sufficiently large F_a can even drive bubbles against buoyancy.

2.3. Bubble contact angles and sliding angles on smart slippery surfaces

For a given smart slippery surface, the bubble contact angle and sliding angle have a crucial role on bubble manipulation. As compiled in Table 1, the contact angles and sliding angles of bubbles on smart slippery surfaces are summarized. Due to the existence of the lubricant, the apparent bubble contact angles are in the range of 45–80°, which is not as large as the bubbles on superaerophobic surfaces.[70] The relatively small bubble contact angles would lead to large contact areas between the bubbles and the slippery surfaces, which is almost always to the disadvantage of bubble manipulation on conventional superwetting surfaces. Fortunately, thanks to the fluidity of the lubricants, most of the smart slippery surfaces demonstrated superior slippery properties with small bubble sliding angles of <15°. The small sliding angles signify small f, making it easy to manipulate bubbles on smart slippery surfaces under external stimuli.

3. Bubble manipulation on smart slippery surfaces

Guided by the above mechanism, various smart slippery surfaces have been designed and prepared by introducing responsive substrates and lubricants to enable bubble manipulation. Typical components include magnetic, photothermal, stretchable, and photopyroelectric substrates, as well as magnetic and phase-transition lubricants.[44–47,80] This permits subtle control of bubble motion under stimuli such as magnetic field, mechanical stretching, light irradiation, and so on. While flexible bubble manipulation has been achieved on smart slippery surfaces under diverse external stimuli, the manipulation modes generally fall into two categories: passive control and active actuation. On tilted smart slippery surfaces, any external stimuli capable of adjusting lateral adhesion—whether increasing or decreasing it—can be harnessed to passively control the bubble movement. In contrast, external stimuli that can yield an actuation force exceeding the lateral adhesion force can be harnessed to actively actuate the bubble on smart slippery surfaces.

3.1. Passive control of bubbles

3.1.1. Magnetic control of bubbles. In general, incorporating magnetic components into the elastic substrates enables facilely modulation of the surface microstructures without altering their chemical composition. By simply exerting magnetic field beneath the slippery surface, the microstructures of the substrate can be deformed, increasing bubble adhesion and pinning bubbles in place. In the absence of a magnetic field, the magnetic-responsive slippery surface remains coated with a continuous lubricant layer, maintaining a slippery state with ultra-low lateral adhesion that permits bubble to slide down an inclined surface. Leveraging this mechanism, in 2019, our group creatively proposed a magnetically reconfigurable slippery gel surface by implanting Fe particles into a PDMS gel with silicone oil as the model lubricant (Fig. 3a).[44] To

Table 1 The bubble contact angles and sliding angles on smart slippery surfaces. "—" denotes no mention in the reference

Materials	Bubble contact angle	Bubble sliding angle	Ref.
Silicone oil infused Fe/PDMS gel	72.4 ± 1.2°	9.2 ± 0.9°	44
Silicone oil infused Co/PDMS/ZnO film	75 ± 1°	~11°	71
Silicone oil infused alumina ceramic slice/tape or rubber	72.8 ± 3.8°	<10°	72
Silicone oil infused micro-grooved PDMS	~54°	<13°	47
Solid paraffin infused Fe_3O_4/PDMS gel film	—	<9°	73
Solid paraffin infused hydroxyapatite nanowires/carbon tube films	—	<15°	74
(Azobenzene)/8CB infused polyRM257 network	~68°	~3°	75
Fluorinated oil infused magnetic microwire array	47.33 ± 2.50°	—	76
Dimethyl silicone oil infused magnetic microplate array	~59.5°	~31.2°	77
Ferrofluid infused laser-ablated surface	75.3 ± 2.5°	—	78
Silicone oil infused PDMS film	—	~3°	46
Silicone oil infused Fe_3O_4/PDMS film	66–80°	<6°	45
Silicone oil infused Prussian blue coated glass	~61°	—	79
Silicone oil infused porous SiO_2/lithium niobate wafer/Fe_3O_4–PDMS film	—	<5°	80

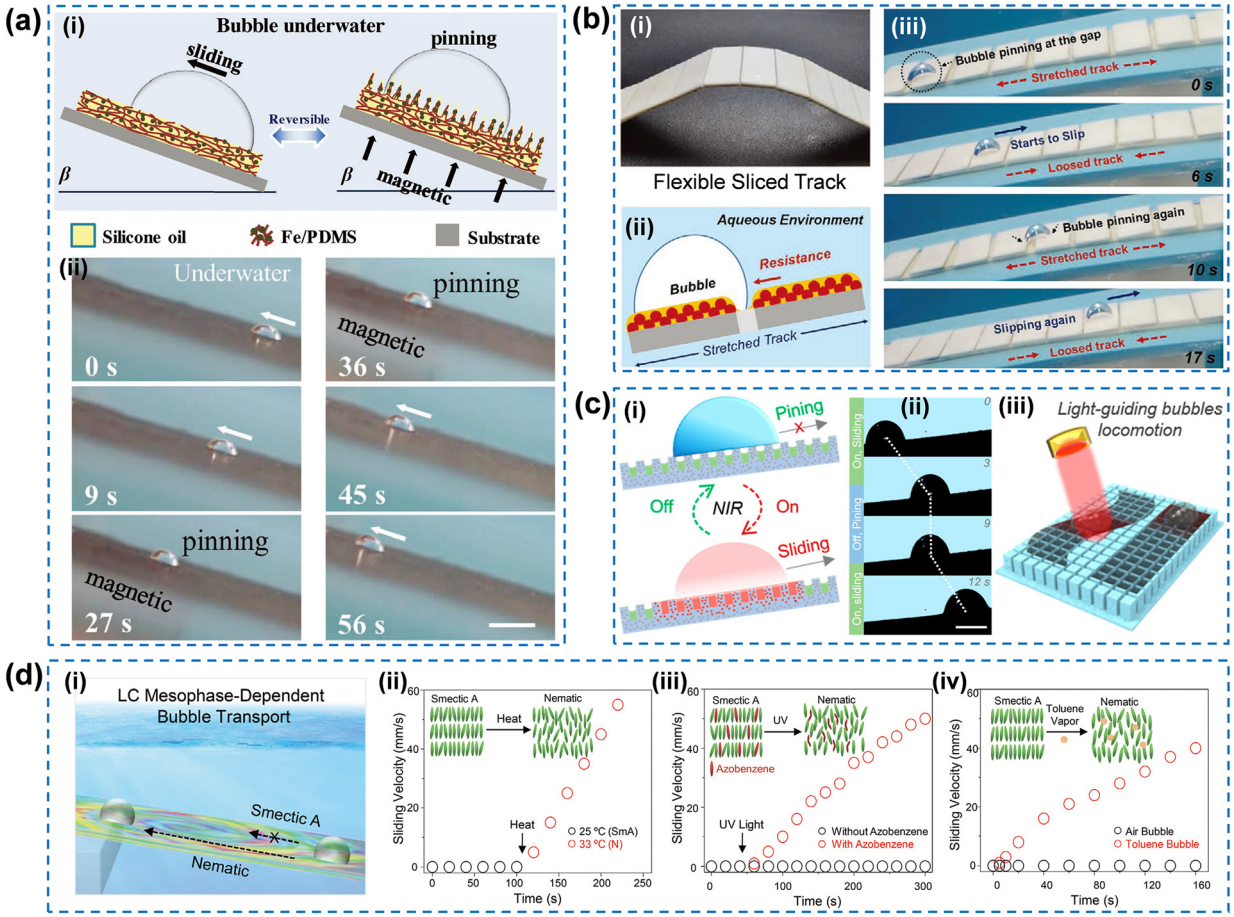

Fig. 3 Passive control of bubbles on smart slippery surfaces under external stimuli. (a) Magnetic manipulation of bubble. (i) Schematic diagram of the reversible formation and disappearance of cones. (ii) Magnetic manipulation of the bubble sliding on the tilted slippery gel surface under a magnetic field, achieving the "slide–pin–slide" motion mode. The scale bar is 5 mm. Reproduced with permission from ref. 44; copyright 2019, WILEY-VCH Verlag GmbH & Co. KGaA, Weinheim. (b) Mechano-stretchable manipulation of the bubble. (i) The digital photo of the substrate. (ii) Schematic demonstration of bubble pining on the stretched slippery surface. (iii) Stretching controllable bubble sliding on the tilted slippery surface. Reproduced with permission from ref. 72; copyright 2021, Wiley-VCH GmbH. (c) Photothermal manipulation of the bubble. (i) Schematic demonstration of NIR manipulation of bubbles on the tilted slippery surface. (ii) Bubble manipulation on the patterned slippery surface. (iii) "Slide–pin–slide" movement mode of the bubble under NIR light. Reproduced with permission from ref. 73; copyright 2021, American Chemical Society. (d) Multi-stimuli manipulation of bubbles. (i) Schematic demonstration of liquid crystal phase-dependent bubble manipulation on a tilted surface. Changes in bubbles' sliding velocities on the 8CB infused slippery surfaces under various stimuli: (ii) temperature, (iii) UV light, and (iv) toluene. The insets are the schematic illustration of phase transition of 8CB between smectic A and the nematic phase under external stimuli. Reproduced with permission from ref. 75; copyright 2022, Wiley-VCH GmbH.

build the slippery surface, the mixture of PDMS precursor, curing agent and Fe particles was intensely stirred. Then, the uniform mixture was coated on a glass substrate with doctor blade method. After curing and infusing silicone oil, the magnetic-responsive slippery gel surface was obtained. Thanks to the low Young's modulus of the elastic PDMS gel,[81] an external magnetic field would uplift magnetic cones on the gel surface, significantly increasing bubble adhesion. After removing the magnetic field, these cones disappear, restoring the surface to its low-adhesion slippery state (Fig. 3a-i). This reversible formation and disappearance of magnetic cones enable a "slide–pin–slide" movement mode for bubbles on the titled slippery gel surface under external magnetic field, as demonstrated in Fig. 3a-ii. Subsequently, Guo's group developed a similar magnetic-responsive slippery surface composed of Co microparticles, PDMS and porous ZnO arrays.[71] By alternately exerting and removing a 0.4 T magnetic field, the magnetic cones irreversibly form and disappear, dynamically regulating the bubble adhesion. Thus, they achieved controllable bubble motion through an external magnetic field.

3.1.2. Mechano-stretchable control of bubbles. Mechanical stretching is a simple but effective method to modulate bubble movement on slippery surfaces. In general, the mechano-stretchable slippery surfaces adopt highly elastic substrates in place of rigid ones.[29,82] Under mechanical stretching, the porous substrates elongate, increasing their surface area. In consequence, the lubricant retracts into the expanded pores, exposing the solid substrates. In this state, the slippery surfaces exhibit high bubble adhesion, pinning

bubble on a slope. When the surface relaxes, a continuous lubricant film fully overspreads the substrate, restoring the low-adhesion state. In this configuration, a bubble deposited on the tilted mechano-stretchable slippery surface can freely slide off. In consideration of these guidelines, inspired by the suspension bridge, Wang and co-workers developed innovative mechano-stretchable slippery tracks based on elastic substrates (Fig. 3b-i).[72] The substrate was constructed by assembling the rigid hydrophobic alumina ceramic slices on flexible tape or elastic rubber. After incorporating silicone oil PMX-200 into the porous structure of the alumina ceramic slices, the mechano-stretchable slippery tracks were successfully yielded. Under elongation, the gaps between the slices widen (Fig. 3b-ii), effectively impeding the bubble movement. Upon dynamic elongating and relaxing, they demonstrated real-time, *in situ* control of bubble sliding on a sloped surface. Similarly, Jiao *et al.* fabricated a mechano-stretchable slippery surface using micro-grooved PDMS surface and silicon oil.[47] The micro-grooved PDMS was prepared by line-by-line laser ablation technology. When applying mechano-stretching, the gaps between the micro-grooves increases, causing the bubble SA to rise from 13° to 90° (firmly pinning on a vertical surface). By alternating stretching and relaxing, they achieved *in situ* dynamic modulation of a bubble movement on a 16° tilted surface.

3.1.3. Photothermal control of bubbles. The use of a photothermal field is another promising strategy for modulating bubble adhesion. Photothermal responsive slippery surfaces for passive bubble manipulation typically employ phase-transition materials as the lubricants and photothermal components as substrates. Typical phase transition materials include solid paraffin, liquid crystals, *etc.*[64,83] Under light irradiation, the substrates convert light into heat, triggering a phase transition of the lubricants into liquid state. Accordingly, this process can significantly reduce the lateral bubble adhesion. For example, Huang *et al.* harnessed femtosecond laser ablation method to fabricate a superhydrophobic Fe_3O_4/PDMS substrate, which was then infused paraffin to create a photothermal slippery surface.[73] Without light irradiation, solid paraffin imparts the surface with high bubble adhesion, pinning the bubbles in place. Upon exposure to NIR light, Fe_3O_4 nanoparticles absorb light and generate heat, rapidly melting the solid paraffin into a liquid state (Fig. 3c-i). Liquid paraffin creates a frictionless surface, allowing bubbles to slide freely on an inclined surface. By switching the NIR light on and off, dynamic bubble positioning is readily achieved in a "slide–pin–slide" mode (Fig. 3c-ii). Using a mask to selectively irradiate the surface with NIR light, they designed patterned slippery surfaces to program bubble sliding pathways. Under masked NIR light irradiation, localized heating converts solid paraffin into liquid, enabling bubbles to spatially navigate along predefined straight line-shaped and tortuous S-shaped tracks (Fig. 3c-iii). This slippery surface also exhibits excellent photothermal self-healing properties. Moreover, Guo's group similarly constructed a patterned photothermal slippery surface adopting paraffin as the model lubricant and a porous hydroxyapatite nanowire/carbon tube film as the photothermal substrate.[74] The substrate film was achieved by filtering the solution composing of hydroxyapatite nanowires, carbon tube and ethanol using a vacuum pump. By combining masks with different patterns, they achieved NIR-manipulating bubble motion along customized pathways.

3.1.4. Multi-responsive control of bubbles. To achieve multi-responsive bubble manipulation on a single surface, slippery surfaces must possess controllable bubble adhesion in response to multiple stimuli, necessitating the integration of multi-responsive substrates and/or lubricants. Following this demand, Rather and co-workers creatively proposed a multi-responsive slippery surface with 8CB liquid crystal as the lubricant and 8CB-swelled porous polyRM257 network as the substrate.[75] The 8CB-swelled porous polyRM257 network was prepared by photo-initiating of the mixture of a liquid crystal, RM257 monomer, and photoinitiator on a functionalized substrate. After infusing (azobenzene)/8CB liquid crystal, they obtained the multi-responsive slippery surface. 8CB possesses intrinsic temperature-dependent mesophases, that is, it assumes a smectic A phase below 25 °C and transfers to the nematic phase when temperature is between 33–44 °C. More interestingly, its mesophases can also be modulated by azobenzene/UV light and toluene. Specifically, adding 5% azobenzene into 8CB enable UV light to induce *cis–trans* isomerization of azobenzene,[84] further triggering the phase transition from a smectic A phase to a nematic phase in 8CB. Moreover, volatile toluene can induce the liquid crystal mesophase transitions.[85] With being in a smectic A phase, 8CB infused slippery surface demonstrates high bubble adhesion of 306 μN, pinning bubbles with low tilted angles. When 8CB transfers to the nematic phase, the bubble adhesion declines to 189 μN, releasing the bubbles to slide (Fig. 3d-i). Building on these mechanisms, Rather and co-workers explored the bubble sliding behaviors in response to temperature, UV light, and toluene. As plotted in Fig. 3d-ii, on a 5° inclined surface, a 10 μL gas bubble is firmly stuck on the surface at 25 °C, whereas heating the surface to 33 °C induces bubbles to rapidly move upward. Furthermore, employing azobenzene/8CB as the lubricant, a 10 μL gas bubble on a 10° inclined surface can be triggered for sliding *via* UV light irradiation (Fig. 3d-iii). Afterwards, they also investigated the sliding behavior of an air bubble containing toluene vapor on a 30° inclined surface. As toluene vapor diffuses into 8CB, it transitions to the nematic phase, consequently activating bubble sliding.

The above four approaches represent the primary types of slippery surfaces capable of modulating bubble adhesion for passive bubble manipulation. While typical examples of each stimulus-responsive approach have been discussed, their unique features warrant comprehensive summarization. To this end, the key characteristics of smart slippery surfaces for passive bubble manipulation are compiled in Table 2.

Table 2 Key features of the typical smart slippery surfaces for passive bubble manipulation

Stimulus types	Working mechanism	Advantages	Disadvantages	Ref.
Magnetic field	Under magnetic field, the reversible formation and appearance of magnetic cones could regulate bubble adhesion	Noncontact, real-time mode	Need low-modulus substrates and strong magnetic field	44 71
Mechanical stretching	Upon mechano-stretching, reversible expanding/retracting the substrate would regulate the lubricant thickness and bubble adhesion	Simple, effective manipulation strategy. Real-time mode	Require elastic substrates with excellent mechanical properties. Contact mode	72 47
Photothermal field	Under NIR light, the melting/solidifying of phase-transition lubricants would modulate bubble adhesion	Remote, noncontact manipulation strategy	Hysteresis between NIR light irradiation and phase transition of lubricants may exist	73 74
Multi-stimuli	In responsive external stimuli (temperature, UV light, and toluene vapor), the transition between the smectic A phase and nematic phase could result in controllable bubble adhesion	Noncontact, multi-responsive strategy. Strong adaptability in applications	Specific lubricants or substrates with multi-responsive properties are needed	75

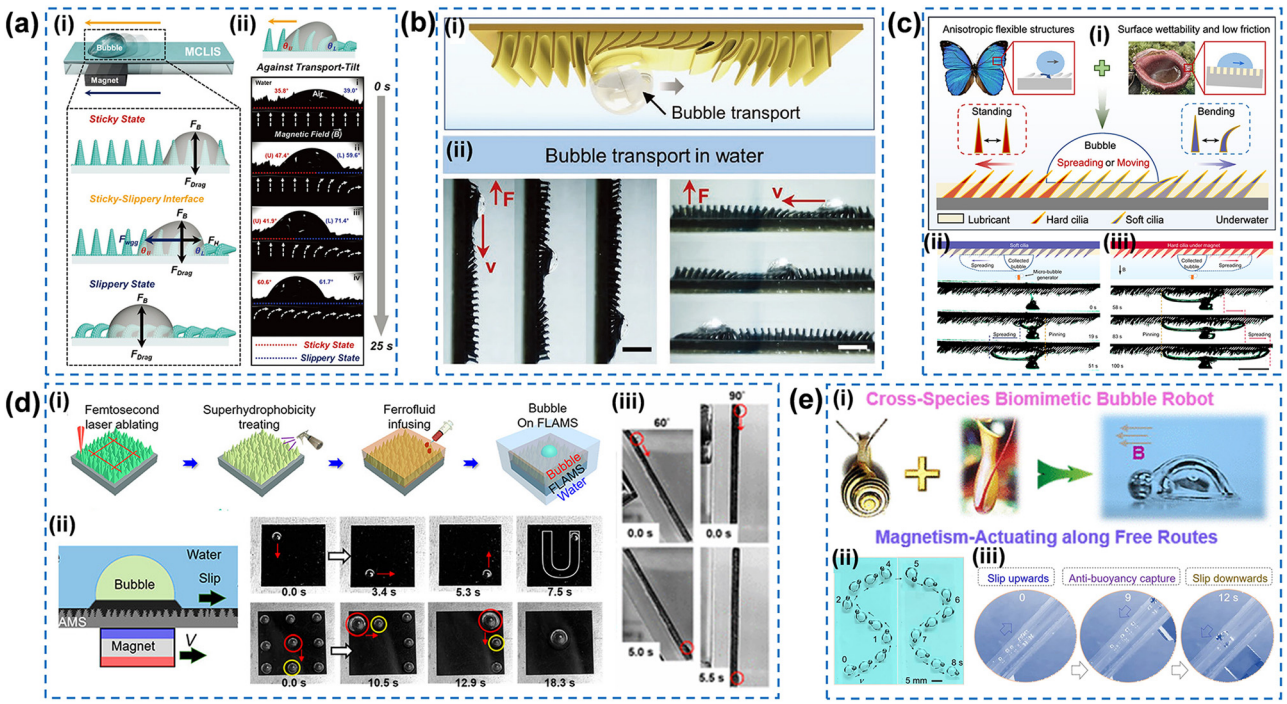

Fig. 4 Magnetic actuation of bubbles on slippery surfaces. (a) Active actuation of the bubble on a magnetic slippery microwires surface. (i) Schematic drawing of the bubble adhesion behaviors on the surfaces under a magnetic field, from top to bottom: sticky state, sticky–slippery interface (bubble moving), and slippery state. (ii) Bubbles moving on the surfaces against the wires. Reproduced with permission from ref. 76; copyright 2021, Wiley-VCH GmbH. (b) Active actuation of the bubble on a magnetic slippery microplate array. (i) Schematic diagram of the bubble transportation. (ii) Magnetic actuation of the bubble movement on the vertical surface (left) and horizontal surface (right). The scale bars are 2 mm. Reproduced with permission from ref. 77; copyright 2022, Wiley-VCH GmbH. (c) Magnetic regulation of bubble spreading on an anisotropically slippery cilia array. (i) The design of the anisotropically slippery cilia array. Bubble transportation (ii) along and (iii) against the tilt direction of the cilia (ii) without and (iii) with a magnetic field, respectively. The scale bar is 1 cm. Reproduced with permission from ref. 87; copyright 2022, American Chemical Society. (d) Active actuation of the bubble on a magnetic fluid infused surface. (i) Schematic showing the fabrication process of the ferrofluid infused slippery surface. (ii) A magnet driving the bubbles in arbitrary directions. (iii) Anti-buoyancy movement of the bubbles on inclined and vertical surfaces. Reproduced with permission from ref. 78; copyright 2020, American Chemical Society. (e) Magnetic robot actuating the bubble on a slippery surface. (i) Design of magnetic actuation of the bubble with a robot on the slippery surface. (ii) Magnetic actuation of the bubble along a programmable "Ω" route. (iii) Magnetic actuation of the bubble anti-buoyancy movement. Reproduced with permission from ref. 46; copyright 2022, American Chemical Society.

3.2. Active actuation of bubbles

3.2.1. Magnetic actuation of bubbles. As a reversible, instantaneous, powerful, and non-contact mode, magnetic actuation of bubbles could be facilely achieved by elaborately creating magnetic responsive slippery surfaces. These surfaces typically integrate magnetic micro-wire/plate arrays as the substrates, ferrofluids as the lubricants, or a magnetic

robot within the bubble.[46,76–78] As illustrated in Fig. 4a, Yong's group implemented the active actuation of bubbles *via* magnetic bending the microwires of a magnetocontrollable lubricant-infused surface (MCLIS).[76] The magnetic substrate was built by coating the mixture of a PDMS precursor, curing agent and cobalt particles on a glass substrate. After curing the substrate on a magnet, a magnetic substrate with microwires was constructed. Following the infusion of fluorinated oil, an MCLIS was obtained. Upon altering the magnetic field position, the bubble on the surface renders three states (Fig. 4a-i). To put concretely, when the microwires are upright, the surface remains a sticky state with high bubble adhesion (~515.83 μN). By completely bending the microwires, the surface transitions to a slippery state with low bubble adhesion (~427.48 μN). In both the sticky state and slippery state, the contact angles on either side of the bubble are equal, maintaining the bubble stationary in an equilibrium state. When the bubble is positioned at the interface between sticky and slippery domains, the contact angle on the sticky side is larger than that on the slippery side. This creates a wettability gradient force (F_{wgg}) that would actuate the bubble to move (Fig. 4a-i). By moving the magnetic field, the bubble can be steered to travel from the slippery domain to the sticky domain (Fig. 4a-ii). In comparison with the conventional slippery surface, this magnetic responsive slippery surface enables effortless anti-buoyancy movement under external magnetic field. Similarly, Shao and co-workers proposed a slippery magnetic microplate array for bubble actuation.[77] They fabricated the magnetic microplate array by curing the mixture of PDMS/curing agent/carbonyl iron powder in a polytetrafluoroethylene plate with groove array. By applying a magnetic field, the microplates bend to form a continuous slippery surface. When continuously maneuvering the magnet field, the actuation force induced by microplate rebounding would drive the bubble (Fig. 4b-i). Due to the large curvature of the bending microplates, anti-buoyancy bubble transportation is realized on a vertical slippery surface (Fig. 4b-ii). Furthermore, the nature structure also inspires us to manipulate bubble movement with a switchable direction on a smart slippery surface. As is well known, butterfly wings with overlapping scales demonstrate anisotropic flexible structures, which endow them with anisotropic bubble adhesion (Fig. 4c-i).[86] With cross-species inspiration from butterfly wings and *Nepenthes* pitcher plants, Yu's group developed a bioinspired magneto-responsive slippery cilia array with switchable bubble directional transportation.[87] The substrate was built by curing the PDMS (containing curing agent) and cobalt particles in a mold with tapered holes. After peeling off, the cilia were coated with poly(methyl methacrylate) powders and hydrophobic lubricant. As shown in Fig. 4c-i, the soft cilia would become hard under an external magnetic field. Without a magnetic field, as microbubbles gradually accumulate on the surface, the growth bubble would transport along the cilia's tilt direction (Fig. 4c-ii). After exerting a magnetic field, the hardened cilia pierced the bubble instead of bending, reversing the bubble transportation direction (Fig. 4c-iii).

Apart from the magnetic substrates, ferrofluids are another effective component for magnetic actuation of bubbles on slippery surfaces. For example, Zhu *et al.* adopted ferrofluid as the lubricant to magnetically steer the bubbles underwater.[78] The ferrofluid is prepared by modifying Fe_3O_4 with oleic acid and then dispersing it into octane. Then, they infused the ferrofluid into a laser-ablated micro-structured surface (Fig. 4d-i). Under an external magnetic field, the oil meniscus around the bubble shrinks.[88] As the magnetic field moves, the bubble can track the magnet's motion at an appropriate speed. Notably, once the magnet's velocity exceeds 25 mm s^{-1}, a 2 μL bubble cannot keep up. With the flexible movement direction of the magnet, the bubbles are steered to travel in freestyle (Fig. 4d-ii). Moreover, sequential merging of nine bubbles is performed by virtue of the flexible magnet (Fig. 4d-ii). In addition, this magnetic actuation method is also capable of driving the bubble against buoyancy at any angles (Fig. 4d-iii). Building upon the existing results, they subsequently infused the ferrofluid into anisotropic micro-grooved surface to achieve directional bubble manipulation.[89] Under an external magnetic field, the bubbles exhibit anisotropic transportation behaviors. Similarly, Guo's group developed a slippery magnetic track using Fe particles and lubricants.[90] Upon exerting a magnetic field, Fe particles undergo a self-assembly into microrods, which will tilt with inclining the magnet. Once the magnet continuously rotates, the microrods swing, driving the bubbles to move forward.

Additionally, dominating magnet robots to steer bubbles is a straightforward yet effective approach.[46] For example, taking inspiration from the decreased moving friction of snail crawls—inducing by the secreting mucus from its pedal gland, and the slippery property of *Nepenthes* pitcher plants, Chen *et al.* employed a bubble-affinitive steel bead to actuate bubbles on a slippery surface (Fig. 4e-i).[46] As demonstrated in Fig. 4e-ii, as the magnetic field is programmatically maneuvered, the bubbles can be accurately guided along designed routes, such as "Ω" – shaped pathway. Leveraging this agile actuation, bubble coalescence can be achieved in arbitrary way. Moreover, on a 45° tilted surface, the magnetic robot can readily navigate the bubble to slide in an anti-buoyancy direction under a moving magnetic field (Fig. 4e-iii). To improve the maneuverability, Guo's group exquisitely engineered superhydrophobic and Janus steel balls with larger dimensions, combined with a solid slippery surface, for steering bubbles underwater.[91] The bubble can be steered to move in an arbitrary direction on a horizontal surface and slide downhill along the anti-buoyancy direction on an inclined surface. Under an external magnetic field, the superhydrophobic and Janus steel balls achieve maximum maneuverable bubble volumes of 1100 and 500 μL, and maximum bubble transportation velocities of 150 and 130 mm s^{-1}, respectively, demonstrating excellent manipulation capacities.

3.2.2. Photothermal actuation of bubbles. As a remote, noncontact, efficient and versatile strategy, NIR light has aroused significant interest for regulating fluid's movement behaviors.[92,93] In the case of bubble actuation, NIR responsive slippery surfaces generally leverage photothermal or photopyroelectric effects. In photothermal scenarios, photothermal components are needed to construct slippery surfaces. When NIR light irradiates on one side of a bubble, local temperature rise can result in a wettability gradient, which guides the bubble movement. By virtue of the above mechanism, Chen *et al.* achieved the NIR-triggered bubble transportation on slippery Fe_3O_4-doped surfaces.[45] The photothermal substrate was prepared by curing the PDMS (containing curing agent) and Fe_3O_4 powders and subsequently laser ablation. Under unilateral NIR light irradiating on the surface, the local surface temperature ascends, reducing the lubricant's surface tension (γ_{OG}). As a result, the contact angle of θ_A decreases ($\theta_A' < \theta_A = \theta_R$, Fig. 5a-i), generating Young's force due to the wettability gradient:[94] $F_{wer\text{-}grad} = \gamma \times A \times (\cos\theta_A' - \cos\theta_R)$, where γ is the water's surface tension and A is the bubble's character length. $F_{wet\text{-}grad}$ would propel the bubble in arbitrary directions by adjusting the NIR light position. Fig. 5a-ii shows the NIR light actuation of the bubble from left to right. Furthermore, when the $F_{wet\text{-}grad}$ overcomes the buoyancy and resistance forces, NIR-triggered anti-buoyancy bubble movement became feasible (Fig. 5a-iii). Therefore, on-demand bubble moving uphill/downhill could be breezily conducted upon toggling the NIR light. After this verification, Qian and coworkers developed a photothermal slippery surface based on a graphene/polyimide membrane, achieving similar NIR actuation of bubbles.[95] This photothermal membrane was fabricated by electrostatic spinning and imidization treatment of polyamide acid to produce a polyimide film, and further laser-induced graphitization of the polyimide film. However, the opaque nature of traditional black photothermal materials seriously limits their application in optical devices. To circumvent this obstacle, Guo's group creatively engineered a transparent photothermal slippery surface by electrostatically assembling Prussian blue (PB) nanocubes onto an etched glass substrate.[79] As shown in Fig. 5b-ii, the PB-coated glass substrates maintain high optical transparency. After exposure to NIR light (Fig. 5b-i), the bubbles can be multi-directionally propelled to transport (Fig. 5b-iii).

3.2.3. Photopyroelectric actuation of bubbles. In addition to direct photothermal actuation, the photopyroelectric effect —capable of generating local nonuniform dielectrophoresis force under NIR light irradiation—also contributes to active bubble actuation. For example, Liu's group innovatively

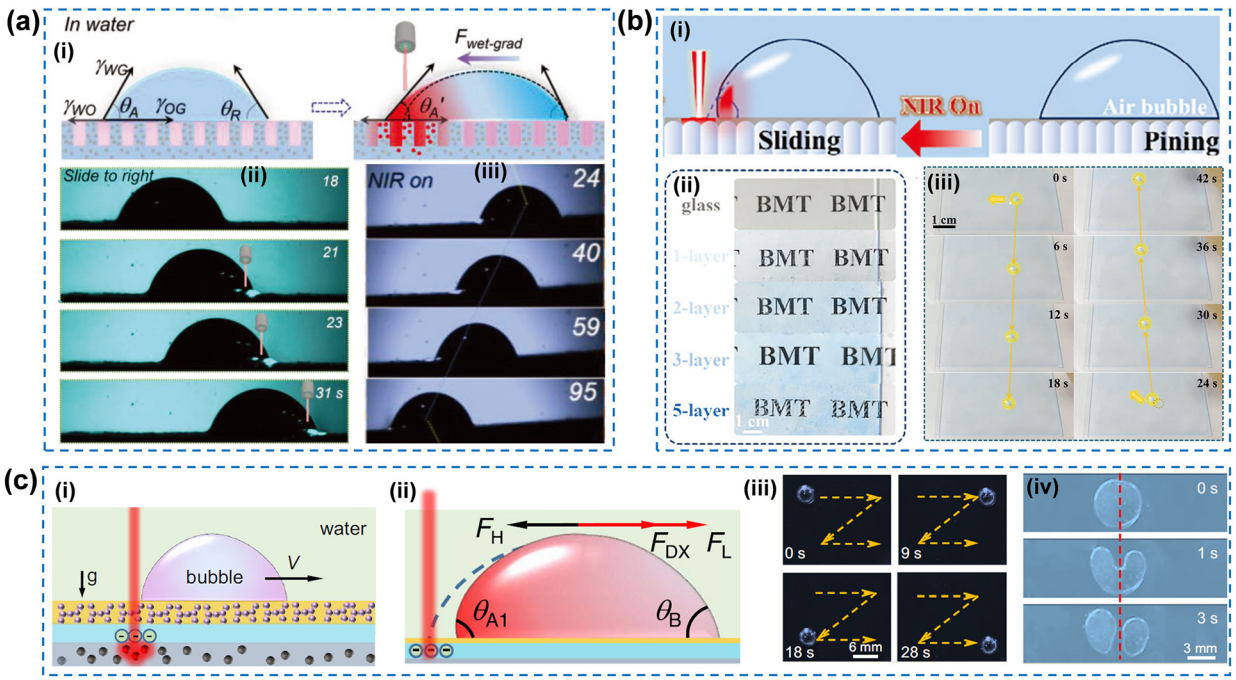

Fig. 5 Actuation of bubbles on slippery surfaces under external stimuli. (a) Photothermal actuation of bubbles. (i) Schematic illustration of the underlying mechanism of photothermal actuation of the bubble on the slippery surface. (ii) Photothermal actuation of the bubble. (iii) Anti-buoyancy movement of the bubble on the slippery surface with a tilt angle of 6°. Reproduced with permission from ref. 45; copyright 2019, WILEY-VCH Verlag GmbH & Co. KGaA, Weinheim. (b) Photothermal actuation of bubbles on a transparent slippery surface. (i) Schematic diagram of the actuating bubble under NIR. (ii) The digital photos of the photothermal substrates with various layers of photothermal materials. (iii) Bubble movement under a NIR trigger. Reproduced with permission from ref. 79; copyright 2024, Wiley-VCH GmbH. (c) Actuating bubbles on photopyroelectric slippery surfaces. Schematic demonstration of (i) the photopyroelectric slippery surface and (ii) NIR-triggered bubble motion. (iii) Bubble movement along a "Z" trajectory. (iv) NIR-induced segmentation of a compressed bubble. Reproduced under terms of the CC-BY license from ref. 80; copyright 2023, the authors, published by Springer Nature.

developed a photopyroelectric slippery surface for multi-behavioral bubble manipulation.[80] The photopyroelectric slippery surface features a sandwich structure: a slippery top layer, a lithium niobate wafer pyroelectric layer, and a Fe_3O_4/PDMS photothermal layer (Fig. 5c-i). The slippery layer was prepared by spraying hydrophobic SiO_2 nanoparticles on the lithium niobate crystal wafers and then spin-coating silicone oil. Upon exposure to NIR light, the local temperature rise diminishes the spontaneous polarization intensity of the lithium niobate wafer, inducing extra surface charges and generating a nonuniform electric field (Fig. 5c-ii).[96,97] Thus, the bubble undergoes a dielectrophoretic force (F_{DX}). This force causes the bubble to shrink, leading to a larger left contact angle (θ_{A1}) than the right contact angle (θ_B) and yielding a Laplace force (F_L). When the resultant force of F_{DX} + F_L surpasses the hydrodynamic resistance force F_H, the bubble would move forward. Harnessing NIR light, the bubble can be actuated along with various pathways, such as a "Z"-shaped trajectory (Fig. 5c-iii). Notably, with the aid of a transparent slippery surface, the compressed bubble could be split under NIR light (Fig. 5c-iv). More intriguingly, NIR light can readily detach the bubbles from the photopyroelectric slippery surfaces by reducing the normal bubble adhesion.

The smart slippery surfaces discussed above exemplify the primary approaches for active bubble actuation. These active strategies offer greater flexibility compared to the passive methods. Each active strategy carries distinct advantages and disadvantages, which require comprehensive understanding by comparison. To this end, Table 3 summarizes the key attributes of the typical active strategies, including the work mechanism, their advantages and disadvantages, and actuation force.

Generally speaking, external stimuli own different advantages and disadvantages of manipulating bubbles on smart slippery surfaces. As for magnetic field-responsive slippery surfaces, they show huge advantages in real-time and remote control of bubbles' movement in passive and active modes due to the strong magnetic force. However, the fine regulation of bubble wettability and adhesion needs further exploration. Mechanical stretching is a simple yet effective strategy to regulate the lubricant thickness and passively control the bubble movement, but it is difficult to actively actuate bubbles under mechanical stretching. Photothermal field and photopyroelectric field have an aptitude for remote and fine regulation of bubble adhesion and wettability, making them promising methods for bubble manipulation. Unfortunately, hysteresis exists between light irradiation and temperature rise, leading to the difficulty of real-time control of bubble's movement. To meet the requirements of various application scenarios, novel materials should be integrated into smart slippery surfaces to achieve the effective, real-time, remote, and fine manipulation of bubbles.

4. Emerging applications

Bubble manipulation, especially in a controllable manner, is of importance for diverse applications ranging from sensors, microfluidic devices, and energy to wastewater treatment.[7,98,99] In recent years, remarkable progress has been made in smart slippery surfaces capable of manipulating bubbles in passive and active strategies. The flexible bubble manipulation capacity endows these surfaces with strong integrating potential in various intelligent

Table 3 The comparison of the typical smart slippery surfaces for active actuation of bubbles

Stimulus types	Working mechanism	Advantages	Disadvantages	Actuation force (F_a)	Ref.
Magnetic field	(1) The rebounding of bending microwires/plates would drag or propel bubbles under a moving magnet	Strong actuation force. Noncontact, real-time mode	Require elastic substrates and strong magnetic field to bend the microwires/plates	Geometry-gradient force (F_{wgg})	76
				Resilience force of the microplate array	77
	(2) The bubble is dragged by the moving ferrofluid under a magnet	Strong actuation force. Noncontact, real-time mode. Relative weak magnetic field	Complex preparation of ferrofluid. The ferrofluid is prone to loss under a dynamic magnet	Magnetic force exerted on the ferrofluid to drag the bubble	78, 89
	(3) Magnetic aerophilic/Janus steel balls pull bubbles on the slippery surface under a moving magnet	Strong actuation force. Noncontact, real-time mode. No special requirement for the slippery surfaces	When the ball is removed, inevitable bubble residue would stick on the ball. Lossless transportation is difficult to achieve	Magnetic force exerted on the steel bead to drag the bubble	46, 91
Photothermal field	Under NIR light illumination, the decline induced by temperature rise would result in a wettability gradient force, propelling the bubble movement	Remote, noncontact mode	Relative weak actuation force. Hysteresis may exist between the light irradiation and response	Wettability gradient force ($F_{wet\text{-}grad}$)	45
				Wettability gradient force	79
Photopyroelectric field	After exposure of NIR light, local temperature rise would bring about nonuniform dielectrophoresis force, which can actuate the bubbles	Remote, noncontact mode. Strong actuation force	Hysteresis may exist between the light irradiation and response	Resultant force of the Laplace force (wettability gradient force) F_L and dielectrophoretic force F_{DX}	80

platforms, underscoring their high promise for future advancements. At present, smart slippery surfaces have been integrated into a myriad of novel devices, including programmable bubble collectors, controllable bubble microreactors, intelligent optical shutters, and flexible bubble microrobots.[44–47,80]

4.1. Bubble collectors

In microfluidic devices, liquid-transport tubes, and submerged gas-generating devices, bubble accumulation could bring about huge puzzles.[100–102] Therefore, effective approaches for collecting the accumulated bubbles are highly desired. Integrating smart slippery surfaces with programmable bubble collection and removal into these devices has been a promising strategy for surmounting the bubble accumulation issue. For instance, Chen and coworkers employed NIR light to manipulate bubbles, and achieved the on-demand bubble collection of a bubble array on a photothermal slippery surface (Fig. 6a).[45] To enhance the collection efficiency, Chen *et al.* mounted an aerophilic steel bead within a bubble to collect bubbles on a slippery surface.[46] As shown in Fig. 6b, by steering the magnetic field, the steel bead drags the bubble to be in contact and emerge with other dispersed bubbles, similar with a "gluttonous snake". Similarly, a Janus steel ball can also be used to collect bubbles on a slippery surface along a specified pathway (Fig. 6c).[91] In addition to collecting the accumulated bubbles, smart slippery surfaces can also be integrated into gas-generating reactions for collecting the bubbles. For example, Wang and co-workers integrated a mechano-stretchable slippery surface into gas mining to achieve spontaneous bubble collection.[72] As illustrated in Fig. 6d, they implanted organic methylene chloride into a pile of quartz sand to simulate flammable ice undersea. Moreover, a heater is mounted under the slippery surface to convert methylene chloride from liquid state to gas state. Upon heating, ceaseless bubbles are generated, collected, and then self-transported on the surface (Fig. 6e). Similarly, Guo's group integrated a magnetic slippery surface into an underwater O_2 generation reaction from H_2O_2 solution, enabling effective bubble collection and delivery.[90]

With rapid and programmable manipulation of bubbles on smart slippery surfaces, it paves a promising avenue for designing and developing novel bubble collectors for gas-producing reactions, gas mining, and so on. However, how to improve the bubble collection efficiency by real-time, finely and precisely regulating the bubble wettability of the smart slippery surfaces under external stimuli remains a great challenge.

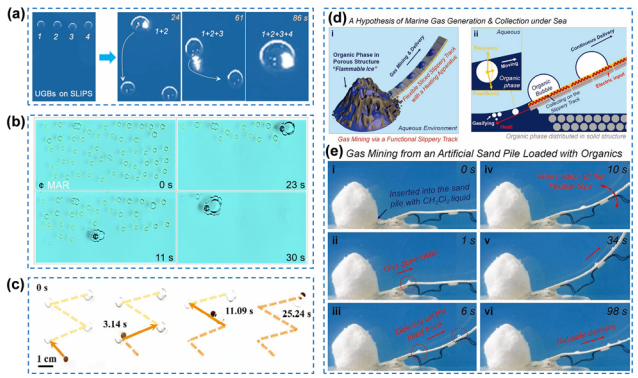

Fig. 6 Programmable bubble collectors based on smart slippery surfaces. (a) Photothermal collection of bubbles. Reproduced with permission from ref. 45; copyright 2019, WILEY-VCH Verlag GmbH & Co. KGaA, Weinheim. (b) Magnetic collection of dispersed bubbles with a magnet robot similar with the "gluttonous snake" game. Reproduced with permission from ref. 46; copyright 2022, American Chemical Society. (c) Magnetic actuation of bubble collection with a Janus magnet ball along the programmed trajectory. Reproduced with permission from ref. 91; copyright 2024, Wiley-VCH GmbH. (d) Schematic diagram of gas mining underwater. (e) Gas mining process containing bubble generation and collection on a mechano-stretchable slippery surface. Reproduced with permission from ref. 72; copyright 2021, Wiley-VCH GmbH.

4.2. Gas reactors

Due to flexible bubble manipulation capacity, smart slippery surfaces hold vast promise for constructing controllable bubble microreactors that are capable of precise steering of reactant bubbles. These smart microreactors could transport the bubbles to a specified location, then the bubbles merge and react.[45,76] For instance, our group achieved the controllable bubble merging on a magnetic responsive slippery surface.[45] As demonstrated in Fig. 7a, a magnet is installed under the inclined slippery surface, leading to the formation of magnetic cones with high bubble adhesion. Therefore, after depositing on the surface, bubble A would be pinned at the interface between high- and low-adhesion regions. Depositing bubble B on the low-adhesion region, it

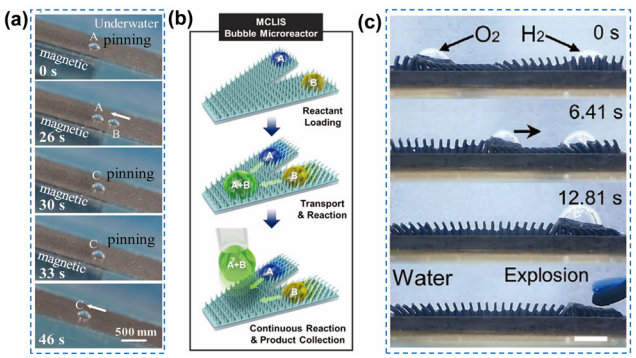

Fig. 7 Controllable gas reactors based on smart slippery surfaces. (a) Magnetocontrollable bubble merging on a 20° titled slippery surface. Reproduced with permission from ref. 44; copyright 2019, WILEY-VCH Verlag GmbH & Co. KGaA, Weinheim. (b) Magnetic actuation of successive bubbles on the two branches of the slippery surface. Reproduced with permission from ref. 76; copyright 2021, Wiley-VCH GmbH. (c) Magnetic driving H_2 and O_2 bubbles coalescence for the reaction. Reproduced with permission from ref. 77; copyright 2022, Wiley-VCH GmbH.

would move toward bubble A. Subsequently, bubbles A and B contact and merge to form bubble C. After withdrawing the magnet, bubble C would slide off the surface freely, demonstrating superior bubble controllability for bubble reaction. Moreover, on horizonal slippery surfaces with active bubble actuation capacity, controllable bubble reaction can also be performed. Han and coworkers validated the feasibility of bubble microreaction on a magnetic slippery surface featuring two branches.[76] As illustrated in Fig. 7b, bubbles A and B are loaded on the two branches, respectively. Upon moving a magnet, the bubbles would move toward the junction, where the two bubbles become in contact and coalesce for the reaction. On this prototype reactor, a representative gas chemical reaction is performed by controlling HCl and NH_3 bubbles to form NH_4Cl, demonstrating programmable chemical synthesis. Another example of a bubble microreactor based on active actuation of bubbles is proposed by Shao and coworkers.[77] On a magnetic slippery microplate array, they deposited an O_2 bubble on the left side and a H_2 bubble on other side. With the help of a moving magnetic field, the rebounding of the bent microplates propels the O_2 bubble to transport toward the H_2 bubble. After merging, the mixed bubble is ignited using an electric spike, inducing an explosive reaction.

Based on the fine and reversible control of bubble movement under external stimuli, smart slippery surfaces have been designed to be gas reactors, which are achieved by separately manipulating bubbles to the designated location. However, escape is inevitable during the manipulation of large bubbles due to the limited bubble adhesion; more reliable and robust gas reactors are highly desired for practical applications in microfluidics and sensors.

4.3. Optical shutters

Due to the ability to scatter and block laser light of bubbles, smart slippery surfaces have been applied to design optical shutters.[73,89] In the case of no bubble in the light path, the laser can pass through freely, keeping the shutter in an open state. When a bubble is steered and pinned on the light path, it would block the light transportation, closing the shutter (Fig. 8a-i).[76] By precisely regulating the bubble position, on-demand optical shutters can be developed based on smart slippery surfaces. Fig. 8a demonstrates a typical paradigm of the bubble shutter based on a slippery magnetic microcilia array.[76] Initially, two bubbles are deposited on the two branches of the surface, allowing the laser light to pass through the central region between the two bubbles. At this point, the laser shows dazzling light intensity. Upon propelling the bubbles to coalesce at the junction of the branches, the merged bubble blocks and scatters the laser light, turning off the light path. The light intensity of the scattered laser is detected to be 77.8% attenuation in comparison with that in the open state. Similarly, Chen *et al.* conducted remote switching of an optical shutter on a photothermal slippery surface using NIR light (Fig. 8b).[45] More interestingly, the limber maneuverability allows the slippery surface to simultaneously modulate multiple bubbles, providing the feasibility of designing multipass optical shutters. As shown in Fig. 8c, they innovatively proposed a three-channel optical shutter.[46] By deliberately manipulating the bubbles to selectively block or release light paths, the laser light can be coded to on-demand signals from (111) to (000) (Fig. 8c-ii).

Thanks to the ability of precisely regulating the bubble location on smart slippery surfaces, optical shutters with flexibility, accuracy, and reusability have been achieved. Such

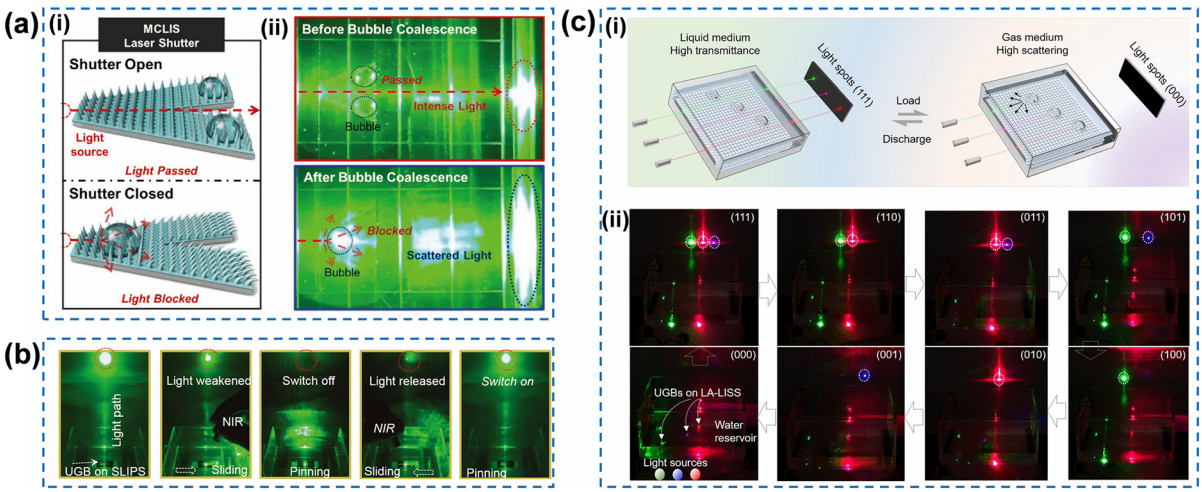

Fig. 8 Intelligent optical shutters based on smart slippery surfaces. (a) Light shutter based on a slippery magnetic microcilia array. (i) Schematic demonstrating the optical shutter. (ii) The change of the light before and after bubble coalescence. Reproduced with permission from ref. 76; copyright 2021, Wiley-VCH GmbH. (b) NIR actuated bubble light shutter. Reproduced with permission from ref. 45; copyright 2019, WILEY-VCH Verlag GmbH & Co. KGaA, Weinheim. (c) Magnetic optical shutter. (i) Schematic demonstrating the turning on/off of the shutter by regulating the bubble position. (ii) Based on magnetic actuation of bubbles, different laser signals are obtained. Reproduced with permission from ref. 46; copyright 2022, American Chemical Society.

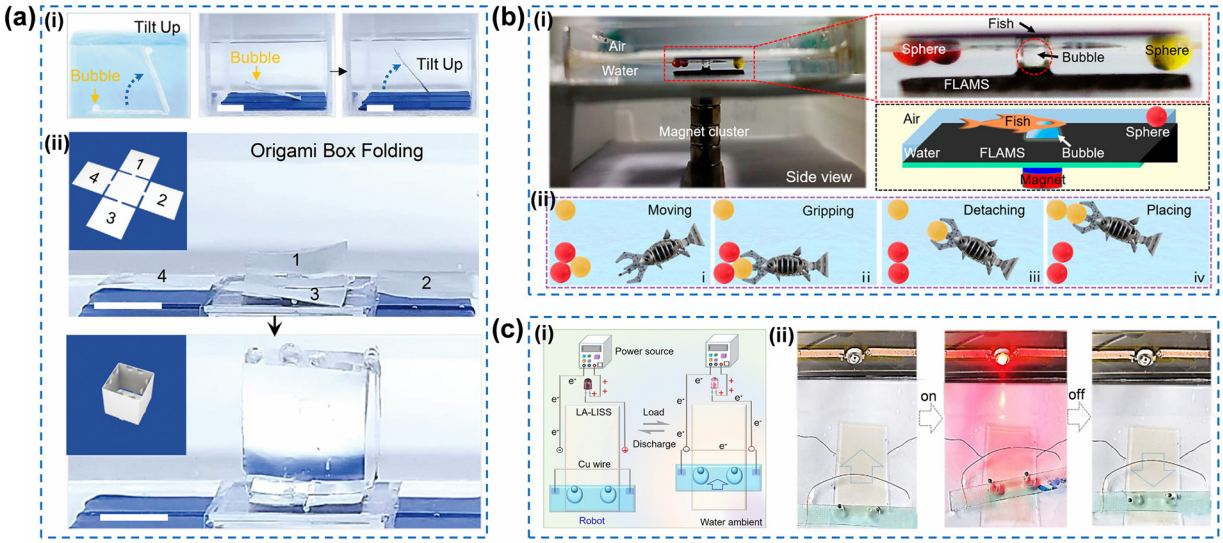

Fig. 9 Flexible bubble microrobots based on smart slippery surfaces. (a) Regulating the object location under buoyancy. (i) A liquid crystal infused aluminum foil is held up by continuous bubble generation. (ii) Complex box folding with bubbles. Reproduced with permission from ref. 75; copyright 2022, Wiley-VCH GmbH. (b) Magnetic bubble microrobot. (i) The experimental setup for towing a plastic fish. (ii) Schematic showing the transfer of polymer balls with the bubble robot. Reproduced with permission from ref. 78; copyright 2020, American Chemical Society. (c) Magnetic bubble microrobot. (i) Schematic diagram of bubble robots steering the copper wire conductors for switching on a circuit. (ii) Switching on/off the circuit with a bubble robot. Reproduced with permission from ref. 46; copyright 2022, American Chemical Society.

intelligent optical shutters verify the huge potential of smart slippery surfaces in areas of optofluidics and optical modulators.

4.4. Bubble microrobots

Artificial robots, serving as mechanical arms and object carriers, have remarkedly motivated the advancement of fields such as the manufacturing industry, electronic information, healthcare industry, and agriculture, thanks to their unique excellent object manipulation capability.[103–105] Smart slippery surfaces with the ability to flexibly manipulate bubbles demonstrate huge potential in object delivery and have been designed to be bubble microrobots. On a smart slippery surface, the objects in contact with bubbles can be accurately harnessed underwater or at the water–gas interface in a remote and noncontact mode. As shown in Fig. 9a, a liquid crystal-infused porous surface demonstrates bubble-powered operations. When the liquid crystal is in a smectic A state, the surface exhibits high bubble adhesion. As continuous CO_2 bubbles form beneath the surface, a liquid crystal infused aluminum foil can be held up when the buoyancy force conquered the foil's gravity (Fig. 9a-i).[75] In this regard, complex box folding can also be carried out submerged (Fig. 9a-ii). In addition, objects with strong bubble affinity can be steered by manipulating bubbles on smart slippery surfaces. As illustrated in Fig. 9b-i, a plastic fish, whose bottom surface is in contact with a bubble on a ferrofluid infused surface, floats at the water–gas interface.[78] By leveraging a moving magnet, the moving bubble tethers and tows the plastic fish, which in turn guides a yellow polymer ball floating on the water (Fig. 9b-ii). Similarly, bubble microrobots can also be used to steer a conductor, such as a piece of copper wire, for switching on a circuit (Fig. 9c-i). As a proof-of-concept demonstration, Chen *et al.* successfully adopted magnetic steel balls to steer bubbles, enabling the controllable movement of a copper wire conductor.[46] As demonstrated in Fig. 9c-ii, when the copper wire bridges the circuit gap, the bulb lights up, underscoring the versatility of bubble microrobots in microscale electrical operations.

Although various bubble microrobots with object manipulation capacity have been developed based on smart slippery surfaces, only tiny objects can be manipulated due to the insufficient actuating force. More powerful smart slippery surfaces with ability to control large objects are still called for further exploration.

As summarized above, smart slippery surfaces have been integrated into bubble collectors, microreactors, optical shutters, and microrobots due to their excellent bubble manipulation capacities whether through passive or active modes. It is envisioned that the progress of multidisciplinary study across materials science and processing technology are poised to drive the development of more multifunctional smart slippery surfaces, thereby expanding the diversity and sophistication of bubble-related devices.

5. Conclusion and perspectives

In this review, we have demonstrated an updated overview of bubble manipulation on smart slippery surfaces, the passive control and active actuation of bubbles under external stimuli, and emerging applications. Following a brief introduction of the design principles of smart slippery surfaces for underwater bubble manipulation, the

fundamental mechanism of passive control and active actuation are discussed. By selecting appropriate responsive substrates and lubricants, versatile smart slippery surfaces have been developed to flexibly manipulate bubbles. We then emphasize the passive control and active actuation of bubbles on these surfaces in response to external stimuli, including magnetic field, photothermal field, temperature, mechanical stretching, and so on. In view of the excellent flexibility and programmability, the emerging bubble-related applications on smart slippery surfaces have been remarkedly highlighted in fields of bubble collectors, microreactors, optical shutters, and microrobots.

In general, current smart slippery surfaces have demonstrated exceptional bubble manipulation capacity in passive or active modes and brought a qualitative leap forward across diverse fields. However, it is worth noting that several severe dilemmas should be surmounted to cater the requirements of future underwater applications. With this aim in mind, the foremost concern of future smart slippery surfaces is long-term stability. Since the advent of slippery surfaces, lubricant loss is an inherent defect.[106] For manipulating bubbles underwater, especially in flowing water, the lubricants in smart slippery surfaces are always subjected to buoyancy and flow-induced shear force,[107] extremely aggravating the lubricant loss, which deteriorates their bubble manipulation function and shortens their intended life. To solve the lubricant loss issue, some potential strategies have been developed, such as constructing nanoscale roughness substrates to enhance the capillary forces between the substrates and the lubricants,[108] preparing gel structures to lock the lubricant,[44] and adopting substrates able to self-replenish lubricants after lubricant loss.[109–112] The above approaches have solved the lubricant loss issue and enhanced the service life of slippery surfaces to some extent, but real-world applications require further improvement. Therefore, more endeavors should be devoted to improve the underwater stability of smart slippery surfaces in the future.

In addition, the multifunctionality of smart slippery surfaces represents another critical consideration. Even though versatile bubble manipulation under external stimuli has been achieved, most current smart slippery surfaces exhibit single-response behavior. Developing multi-responsive slippery surfaces would not only improve the flexibility of bubble manipulation, but also enhance their reliability and adaptiveness in complex underwater scenarios. To this end, the strategic combination of responsive substrates and lubricants, and advanced nanotechnologies like 4D printing hold promise for diversifying the slippery surfaces' functions.

On a final note, in terms of application areas, although current bubble manipulation on smart slippery surfaces has been integrated into innovative fields, unlocking far-ranging application scenarios is still an existing challenge. By virtue of the flexible bubble manipulation, smart slippery surfaces offer vast potential in possible areas such as bubble sensors,[113] smart nanogenerators,[114] gas-involving electrodes, and targeted drug delivery.[115] Moreover, the applications under extreme or special conditions warrant further exploration, such as gas mining in deep sea with ultrahigh pressure, manipulation of airflow for continuous transportation,[41] and gas delivery in turbulent liquids.

Overall, smart slippery surfaces have proven to be promising platforms for bubble manipulation, accelerating the development of a wide range of applications. We envision that future research on smart slippery surfaces for bubble manipulation will concentrate more on opening new frontiers for fundamental research and breaking down the barriers of commercial applications.

Author contributions

Duanqiang Shi: conceptualization, data curation, investigation, methodology, writing – original draft; Pu Guo: conceptualization, data curation, investigation, methodology, writing – review & editing; Yang Liu, Xiaoxiao Zhou, and Shuchun Jiang: data curation, investigation, visualization; Zubin Wang: conceptualization, funding acquisition, project administration, supervision, writing – review & editing; Qun Xu: project administration, supervision, writing – review & editing.

Conflicts of interest

There are no conflicts to declare.

Data availability

No primary research results, software or code have been included and no new data were generated or analysed as part of this review.

Acknowledgements

This work was supported by the National Natural Science Foundation of China (22205215), the China Postdoctoral Science Foundation (2024M762980), the Key Science and Technology Program of Henan Province (222102240119), and the Distinguished Young Researchers' Program of Zhengzhou University (32340148).

References

1 D. C. Upham, V. Agarwal, A. Khechfe, Z. R. Snodgrass, M. J. Gordon, H. Metiu and E. W. McFarland, *Science*, 2017, **358**, 917–921.
2 R. Chen, C. Cheng, Z. Liu, Y. Hu, J. Zhao, Z. Zuo, J. Xu and H. Wang, *Int. J. Heat Mass Transfer*, 2024, **233**, 126005.
3 K. Dong, J. Chen, X. Xia, W. Deng, S. A. Khan, X. Zhang, Y. Zi and J. Zhao, *Nano Energy*, 2024, **131**, 110256.
4 B. Wang, Y. Liu, Y. Zhao, E. Liu, Z. Li and Z. Miao, *Adv. Funct. Mater.*, 2025, **35**, 2507648.
5 L. Zhang, R. Iwata, Z. Lu, X. Wang, C. D. Díaz-Marín and Y. Zhong, *Chem. Rev.*, 2024, **124**, 10052–10111.

6 Q. Shi, H. Zhu, J. Zhu, N. Wu, H. He, W. Lu and Z. Ou, *Fuel*, 2022, **324**, 124744.
7 C. Zhang, M. Cao, H. Ma, C. Yu, K. Li, C. Yu and L. Jiang, *Adv. Funct. Mater.*, 2017, **27**, 1702020.
8 D. Sauter, A. Steuer, K. Wasmund, B. Hausmann, U. Szewzyk, A. Sperlich, R. Gnirss, M. Cooper and T. Wintgens, *Sci. Total Environ.*, 2023, **856**, 159265.
9 C. Yu, P. Zhang, J. Wang and L. Jiang, *Adv. Mater.*, 2017, **29**, 1703053.
10 M. Li, P. Xie, L. Yu, L. Luo and X. Sun, *ACS Nano*, 2023, **17**, 23299–23316.
11 Y. Hu, Z. Xu, H. Shi, B. Wang, L. Wang and L.-W. Zhang, *Nat. Commun.*, 2025, **16**, 3682.
12 Y. Du, P. Li, Y. Wen and Z. Guan, *Small*, 2023, **19**, 2207256.
13 L. Yu, Y. Yang, P. Xie, Q. Xu, A. Kumar, L. Luo, H. Li, H. Xu, H. Duan and X. Sun, *EES Catal.*, 2025, **3**, 152–160.
14 S. Jeong, U. Kim, S. Lee, Y. Zhang, E. Son, K.-J. Choi, Y.-K. Han, J. M. Baik and H. Park, *ACS Nano*, 2024, **18**, 7558–7569.
15 D. Neumann and D. Woermann, *Springerplus*, 2013, **2**, 694.
16 R. S. Seymour and P. G. D. Matthews, *J. Exp. Biol.*, 2013, **216**, 164–170.
17 H. de Maleprade, C. Clanet and D. Quéré, *Phys. Rev. Lett.*, 2016, **117**, 094501.
18 J. Gao, Q. Ma, Y. Zhang, S. Xue, J. Young, M. Zhao, Z. J. Ren, J.-H. Kim and W. Zhang, *ACS Nano*, 2024, **18**, 10302–10311.
19 S. Liu, P. Chen, T. Yang, P. Wu, C. Liu, J. He and W. Jiang, *Ind. Eng. Chem. Res.*, 2022, **61**, 10955–10968.
20 J. Kim, S. M. Jung, N. Lee, K. S. Kim, Y. T. Kim and J. K. Kim, *Adv. Mater.*, 2023, **35**, 2305844.
21 J. Jiang, G. Xu, B. Gong, J. Zhu, W. Wang, T. Zhao, Y. Feng, Q. Wu, S. Liu and L. Zhang, *Adv. Funct. Mater.*, 2024, **35**, 2412685.
22 Z. Lu, Y. Li, X. Lei, J. Liu and X. Sun, *Mater. Horiz.*, 2015, **2**, 294–298.
23 S. Ben, Y. Ning, Z. Zhao, Q. Li, X. Zhang, L. Jiang and K. Liu, *Adv. Funct. Mater.*, 2022, **32**, 2113374.
24 R. Poetes, K. Holtzmann, K. Franze and U. Steiner, *Phys. Rev. Lett.*, 2010, **105**, 166104.
25 C. Zhang, B. Zhang, H. Ma, Z. Li, X. Xiao, Y. Zhang, X. Cui, C. Yu, M. Cao and L. Jiang, *ACS Nano*, 2018, **12**, 2048–2055.
26 Y. Meng, S. Xing, Z. Weng, S. Wang, X. Yi and N. Wu, *Chem. Eng. J.*, 2023, **476**, 146384.
27 Y. A. Mehanna, E. Sadler, R. L. Upton, A. G. Kempchinsky, Y. Lu and C. R. Crick, *Chem. Soc. Rev.*, 2021, **50**, 6569–6612.
28 T.-S. Wong, S. H. Kang, S. K. Y. Tang, E. J. Smythe, B. D. Hatton, A. Grinthal and J. Aizenberg, *Nature*, 2011, **477**, 443–447.
29 X. Yao, Y. Hu, A. Grinthal, T.-S. Wong, L. Mahadevan and J. Aizenberg, *Nat. Mater.*, 2013, **12**, 529–534.
30 X. Hou, Y. Hu, A. Grinthal, M. Khan and J. Aizenberg, *Nature*, 2015, **519**, 70–73.
31 K. Han, Z. Wang, X. Han, X. Wang, P. Guo, P. Che, L. Heng and L. Jiang, *Adv. Funct. Mater.*, 2022, **32**, 2207738.
32 B. Li, K. Huang, S. Xue, W. Liu and J. Li, *ACS Appl. Mater. Interfaces*, 2025, **17**, 19105–19116.
33 F. Wang, M. Liu, C. Liu, Q. Zhao, T. Wang, Z. Wang and X. Du, *Sci. Adv.*, 2022, **8**, eabp9369.
34 N. Vogel, R. A. Belisle, B. Hatton, T.-S. Wong and J. Aizenberg, *Nat. Commun.*, 2013, **4**, 2176.
35 Z. Wang, L. Heng and L. Jiang, *J. Mater. Chem. A*, 2018, **6**, 3414–3421.
36 H. Zhou, H. Niu, H. Wang and T. Lin, *Chem. Rev.*, 2022, **123**, 663–700.
37 H. Jiang, X. Chen, Z. Fang, Y. Xiong, H. Wang, X. Tang, J. Ren, P. Tang, J. Li, G. Wang and Z. Li, *ACS Appl. Mater. Interfaces*, 2024, **16**, 34089–34099.
38 L. Yin, R. Tan, J. Han, J. Wang, J. Cheng, D. Wu, T. Zhang and L. Wang, *Adv. Sci.*, 2025, e05526.
39 X. Tang, H. Xiong, T. Kong, Y. Tian, W.-D. Li and L. Wang, *ACS Appl. Mater. Interfaces*, 2018, **10**, 3029–3038.
40 D. Gao, C. Li, C. Zhang, B. Yang, J. Gao, X. Si, J. Qi and J. Cao, *Mater. Today Commun.*, 2024, **38**, 107979.
41 X. Wang, H. Bai, Z. Li, Y. Tian, T. Zhao and M. Cao, *Mater. Horiz.*, 2023, **10**, 3351–3359.
42 J. Li and Z. Guo, *Research*, 2019, **2019**, 9139535.
43 C. Yu, X. Zhu, K. Li, M. Cao and L. Jiang, *Adv. Funct. Mater.*, 2017, **27**, 1701605.
44 P. Guo, Z. Wang, L. Heng, Y. Zhang, X. Wang and L. Jiang, *Adv. Funct. Mater.*, 2019, **29**, 1808717.
45 C. Chen, Z. Huang, L. A. Shi, Y. Jiao, S. Zhu, J. Li, Y. Hu, J. Chu, D. Wu and L. Jiang, *Adv. Funct. Mater.*, 2019, **29**, 1904766.
46 C. Chen, H. Yao, Y. Jiao, C. Jia and S. Wu, *Langmuir*, 2022, **38**, 2174–2184.
47 Y. Jiao, Y. Zhang, X. Lv, J. Ji, Z. Wang, Y. Su, X. Liu and K. Liu, *Langmuir*, 2021, **37**, 2140–2145.
48 J. Wang, Z. Guo and F. Fu, *Adv. Colloid Interface Sci.*, 2024, **332**, 103266.
49 D. Liu, Y. Wang, W. Chen, Y. Tian, F. Zhang, S. Wang and J. Meng, *Nano Today*, 2024, **55**, 102177.
50 H. F. Bohn and W. Federle, *Proc. Natl. Acad. Sci. U. S. A.*, 2004, **101**, 14138–14143.
51 U. Bauer and W. Federle, *Plant Signaling Behav.*, 2014, **4**, 1019–1023.
52 Z. Wang, Y. Liu, P. Guo, L. Heng and L. Jiang, *Adv. Funct. Mater.*, 2018, **28**, 1801310.
53 A. Chen, Q. Zeng, L. Tan, T. Wang, F. Xu, J. Wang, X. Tao, Y. Yang and X. Wang, *Adv. Funct. Mater.*, 2024, **34**, 2405698.
54 Z. Wang, Q. Xu, L. Wang, L. Heng and L. Jiang, *J. Mater. Chem. A*, 2019, **7**, 18510–18518.
55 B. Aktaş, R. Jafari and H. Koivuluoto, *J. Therm. Spray Technol.*, 2025, **34**, 1843–1854.
56 M. Zhang, S. Chen, M. Dong and Z. Guo, *Eng. Sci.*, 2018, **3**, 67.
57 D. Chen, B. Wang, X. Yang and M. Zhong, *Adv. Eng. Mater.*, 2023, **25**, 2201732.
58 I.-I. N. Etim, R. Zhang, C. Wang, S. Khan, K. Mathivanan and J. Duan, *npj Mater. Degrad.*, 2025, **9**, 34.

59 G. Tian, J. Wang, H. Su, C. Xue, X. Yang, Q. Li, X. Li, Y. Miao and Z. Yang, *Prog. Org. Coat.*, 2024, **196**, 108696.
60 R. Wang, F. Jin, Y. Li, J. Gong, H. Lai, Y. Liu and Z. Cheng, *Adv. Funct. Mater.*, 2023, **33**, 2305766.
61 X. Han, S. Tan, R. Jin, L. Jiang and L. Heng, *J. Am. Chem. Soc.*, 2023, **145**, 6420–6427.
62 C. Vega-Sánchez and C. Neto, *Langmuir*, 2024, **40**, 4460–4467.
63 S. Rowthu and P. Hoffmann, *ACS Appl. Mater. Interfaces*, 2018, **10**, 10560–10570.
64 Y. Xu, Y. Yao, W. Deng, J.-C. Fang, R. L. Dupont, M. Zhang, S. Čopar, U. Tkalec and X. Wang, *Nano Res.*, 2022, **16**, 5098–5107.
65 Y. Xu, A. M. Rather, Y. Yao, J.-C. Fang, R. S. Mamtani, R. K. A. Bennett, R. G. Atta, S. Adera, U. Tkalec and X. Wang, *Sci. Adv.*, 2021, **7**, eabi7607.
66 P. Che, L. Heng and L. Jiang, *Adv. Funct. Mater.*, 2017, **27**, 1606199.
67 J. Sarma, D. Monga, Z. Guo, F. Chen and X. Dai, *Droplet*, 2024, **3**, e106.
68 H. Zhao, R. Wen, L. Zhang, L. Chen, H. Li, F. Xia and Y. Song, *Adv. Sci.*, 2024, **11**, 2406325.
69 Z. Wang, L. Jiang and L. Heng, *ACS Nano*, 2025, **19**, 13549–13566.
70 J. Ryu and D. W. Lee, *J. Mater. Chem. A*, 2024, **12**, 10012–10043.
71 C. Liu, J. Huang, Z. Guo and W. Liu, *Chem. Commun.*, 2022, **58**, 11119–11122.
72 X. Wang, H. Bai, J. Yang, Z. Li, Y. Wu, C. Yu, L. Jiang and M. Cao, *Small*, 2021, **17**, 2007803.
73 Z. Huang, C. Chen, X. Wang, R. Li, Y. Bian, S. Zhu, Y. Hu, J. Li, D. Wu and J. Chu, *ACS Appl. Mater. Interfaces*, 2021, **13**, 9272–9280.
74 Q. Li, D. Wu and Z. Guo, *Soft Matter*, 2019, **15**, 6803–6810.
75 A. M. Rather, Y. Xu, Y. Chang, R. L. Dupont, A. Borbora, U. I. Kara, J. C. Fang, R. Mamtani, M. Zhang, Y. Yao, S. Adera, X. Bao, U. Manna and X. Wang, *Adv. Mater.*, 2022, **34**, 2110085.
76 K. Han and K. Yong, *Adv. Funct. Mater.*, 2021, **31**, 2101970.
77 K. Shao, S. Jiang, Y. Hu, Y. Zhang, C. Li, Y. Zhang, J. Li, D. Wu and J. Chu, *Adv. Funct. Mater.*, 2022, **32**, 2205831.
78 S. Zhu, Y. Bian, T. Wu, C. Chen, Y. Jiao, Z. Jiang, Z. Huang, E. Li, J. Li, J. Chu, Y. Hu, D. Wu and L. Jiang, *Nano Lett.*, 2020, **20**, 5513–5521.
79 A. Yu and Z. Guo, *Small*, 2024, **20**, 2405878.
80 H. Zhan, Z. Yuan, Y. Li, L. Zhang, H. Liang, Y. Zhao, Z. Wang, L. Zhao, S. Feng and Y. Liu, *Nat. Commun.*, 2023, **14**, 6158.
81 A. Ahmadianyazdi, I. J. Miller and A. Folch, *Lab Chip*, 2023, **23**, 4019–4032.
82 Y. Wang, B. Qian, C. Lai, X. Wang, K. Ma, Y. Guo, X. Zhu, B. Fei and J. H. Xin, *ACS Appl. Mater. Interfaces*, 2017, **9**, 24428–24432.
83 S. Yun, S. Lee and K. Yong, *Nano Energy*, 2024, **129**, 110075.
84 E. Bukusoglu, M. Bedolla Pantoja, P. C. Mushenheim, X. Wang and N. L. Abbott, *Annu. Rev. Chem. Biomol. Eng.*, 2016, **7**, 163–196.
85 W. Hu, J. Sun, Q. Wang, L. Zhang, X. Yuan, F. Chen, K. Li, Z. Miao, D. Yang, H. Yu and H. Yang, *Adv. Funct. Mater.*, 2020, **30**, 2004610.
86 H. Mei, D. Luo, P. Guo, C. Song, C. Liu, Y. Zheng and L. Jiang, *Soft Matter*, 2011, **7**, 10569–10573.
87 C. Zhang, X. Xiao, Y. Zhang, Z. Liu, X. Xiao, A. Nashalian, X. Wang, M. Cao, X. He, J. Chen, L. Jiang and C. Yu, *ACS Nano*, 2022, **16**, 9348–9358.
88 W. Wang, J. V. I. Timonen, A. Carlson, D.-M. Drotlef, C. T. Zhang, S. Kolle, A. Grinthal, T.-S. Wong, B. Hatton, S. H. Kang, S. Kennedy, J. Chi, R. T. Blough, M. Sitti, L. Mahadevan and J. Aizenberg, *Nature*, 2018, **559**, 77–82.
89 Y. Bian, S. Zhu, C. Ye, C. Chen, B. Xu, Y. Zhang, C. Zhang, X. Wang, Y. Hu, J. Li, D. Wu and J. Chu, *Adv. Mater. Interfaces*, 2022, **9**, 2102116.
90 W. Chen, X. Zhang, S. Zhao, J. Huang and Z. Guo, *Chem. Commun.*, 2022, **58**, 1207–1210.
91 Z. Zhao, S. He, A. Yu, S. Wang, H. Zhang and Z. Guo, *Adv. Funct. Mater.*, 2024, **35**, 2418725.
92 X. Jing, H. Chen, X. Shang, L. Zhang, S. Zhao, X. Zhou, X. Liu, Z. Wang, Y. Wang, W. Du, Y. Guo and L. Jiang, *Adv. Funct. Mater.*, 2024, **35**, 2410612.
93 S. Tan, X. Han, Y. Sun, P. Guo, X. Sun, Z. Chai, L. Jiang and L. Heng, *ACS Nano*, 2024, **18**, 8484–8495.
94 C. G. L. Furmidge, *J. Colloid Sci.*, 1962, **17**, 309–324.
95 C. Qian, Z. Chen, X. Meng, Q. Li and X. Chen, *Chem. Eng. J.*, 2023, **469**, 143819.
96 W. Li, X. Tang and L. Wang, *Sci. Adv.*, 2020, **6**, eabc1693.
97 T. B. Jones, *J. Electrost.*, 1979, **6**, 69–82.
98 B. Luo, X. Wang, T. Liu, C. Cai, Y. Liu, S. Zhang, M. Chi, C. Gao, J. Wang, Z. Liu, S. Wang and S. Nie, *Adv. Funct. Mater.*, 2024, **34**, 2315725.
99 M. Prakash and N. Gershenfeld, *Science*, 2007, **315**, 832–835.
100 J. H. Sung and M. L. Shuler, *Biomed. Microdevices*, 2009, **11**, 731–738.
101 R. Liu, J. Huang, J. Li, E. Placidi, F. Chen, X. Zhu and Q. Liao, *ACS Appl. Mater. Interfaces*, 2024, **16**, 33336–33346.
102 Z. Long, C. Yu, M. Cao, J. Ma and L. Jiang, *Adv. Mater.*, 2024, **36**, 2312179.
103 S. Sankar, W.-Y. Cheng, J. Zhang, A. Slepyan, M. M. Iskarous, R. J. Greene, R. DeBrabander, J. Chen, A. Gupta and N. V. Thakor, *Sci. Adv.*, 2025, **11**, eadr9300.
104 W. Li, F. Luo, Y. Liu, Y. Zou, L. Mo, Q. He, P. J. Lin, Q. Xu, A. Liu, C. Zhang, J. Cheng, L. Cheng and L. Ji, *Adv. Mater.*, 2025, **37**, 2419059.
105 J. Qu, B. Mao, Z. Li, Y. Xu, K. Zhou, X. Cao, Q. Fan, M. Xu, B. Liang, H. Liu, X. Wang and X. Wang, *Adv. Funct. Mater.*, 2023, **33**, 2306249.
106 S. Peppou-Chapman, J. K. Hong, A. Waterhouse and C. Neto, *Chem. Soc. Rev.*, 2020, **49**, 3688–3715.
107 C. Howell, T. L. Vu, C. P. Johnson, X. Hou, O. Ahanotu, J. Alvarenga, D. C. Leslie, O. Uzun, A. Waterhouse, P. Kim, M.

Super, M. Aizenberg, D. E. Ingber and J. Aizenberg, *Chem. Mater.*, 2015, **27**, 1792–1800.
108 P. Kim, M. J. Kreder, J. Alvarenga and J. Aizenberg, *Nano Lett.*, 2013, **13**, 1793–1799.
109 J. Cui, D. Daniel, A. Grinthal, K. Lin and J. Aizenberg, *Nat. Mater.*, 2015, **14**, 790–795.
110 H. Zhao, Q. Sun, X. Deng and J. Cui, *Adv. Mater.*, 2018, **30**, 1802141.
111 Q. Rao, J. Zhang, X. Zhan, F. Chen and Q. Zhang, *J. Mater. Chem. A*, 2020, **8**, 2481–2489.
112 H. Zhan, Y. Xia, Y. Liu, H. Sun, W. Ge, S. Feng and Y. Liu, *Adv. Funct. Mater.*, 2023, **33**, 2211317.
113 X. Xue, R. Wang, L. Lan, J. Wang, Z. Xue and L. Jiang, *ACS Appl. Mater. Interfaces*, 2018, **10**, 5099–5106.
114 X. Yan, W. Xu, Y. Deng, C. Zhang, H. Zheng, S. Yang, Y. Song, P. Li, X. Xu, Y. Hu, L. Zhang, Z. Yang, S. Wang and Z. Wang, *Sci. Adv.*, 2018, **8**, eabo7698.
115 J. Jeong, D. Jang, D. Kim, D. Lee and S. K. Chung, *Sens. Actuators, A*, 2020, **306**, 111973.